Atmospheric
Measurement
Techniques
Discussions
Open Access
EGU

SPARCLE 2: A new optical particle counter to measure particle size and refractive index

Moch S. Romadhon[a,c], Dan Peters[b], and Roy Gordon Grainger[a]

[a]Atmospheric, Oceanic and Planetary Physics, Univ. of Oxford, UK.
[b]Rutherford Appleton Laboratory, Science and Technology Facilities Council, UK.
[c]The Research Center for Climate and Atmosphere, National Research and Innovation Agency, Indonesia.

Correspondence: Romadhon, Moch S. (moch.syarif.romadhon@brin.go.id)

Abstract. In the last few decades, there has been an increasing need to improve *in situ* aerosol measurements to better understand the role of atmospheric aerosol on the Earth's climate system and to assess the quality of ambient air. At the moment, *in situ* optically based aerosol photometers assume the refractive index of measured particles to give a size estimate. This assumption can result in large errors in estimated size. This study describes an instrument, called SPARCLE 2, that addresses this problem by simultaneously measuring the particle size and refractive index. SPARCLE 2 has two detectors to measure the pattern of aerosol-scattered light. The first is a detector with high sensitivity and high temporal resolution mainly to detect the presence of particles in the sensing volume. The second is a detector with high angular resolution to capture the pattern of scattered light. SPARCLE 2 is designed to measure particles whose diameters lie in the range 500 nm to 2,500 nm typical of the accumulation mode of troposphere aerosol. A theoretical lower particle size limit of 300 nm is determined by the optical and electronic noise. In practice, stray light limits the lower limit to a particle diameter of 800 nm. SPARCLE 2's accuracy was tested using four monodisperse aerosols formed from non-absorbing polystyrene latex beads. The mean diameters of the test particles were 1,100 nm, 1,800 nm, 2,000 nm and 3,000 nm and their refractive index were 1.59. The standard deviation between SPARCLE 2's measurement and the manufacturer's stated size was 13% for the 1,100 nm size particles and less than 3% for the three larger sizes. The refractive index deviation was less than 1.25% for all sizes. SPARCLE 2 was used to measure ambient Oxford (UK) city air. The size distributions measured by SPARCLE 2 were similar to those measured by a commercial optical particle counter. The refractive index distribution was consistent with the most abundant aerosol compositions around Oxford which are NO_3^-, NH_4^+ and SO_4^{2-}.

1 Introduction

Improved characterisation of *in situ* aerosol properties is needed to better understand the impact of aerosol pollution on the Earth's climate and human health (IPCC, 2014; WHO, 2013). For example, Peters et al. (2001) showed that a few hours exposure to particulate matters of sizes less than 2,500 nm and concentrations higher than $25\,\mu g\,m^{-3}$ may elevate heart attack risk. Other studies confirm the link between particulate matter exposure and cardiovascular morbidity and mortality (Brook et al., 2010, 2004; IARC, 2013). The measurement of aerosol size and refractive index is needed to have a better understanding of how aerosol scattering and absorption impact the Earth's radiative balance (Boucher and Lohmann, 1995; Myhre et al.,

25 2013; IPCC, 2014; Valenzuela et al., 2018). Recent studies show that the lack of confidence in the magnitude of aerosol effects can be partly attributed to the uncertainty in the refractive indices of tropospheric aerosol particles (Erlick et al., 2011; Zarzana et al., 2014; Valenzuela et al., 2018).

In tropospheric aerosol research, optical particle counters (OPCs) are widely used due to their applicability for *in situ*, real time measurement. An OPC estimates particle size using a measurement of particle-scattered light where the particle is assumed

30 to be a homogeneous sphere. The main drawback of OPCs is the need to assume particle refractive index (Szymanski et al., 2009). There are three recently developed designs of OPCs to tackle this drawback. The first is an OPC that measures two-dimensional angular optical scattering over large scattering angles (Aptowicz et al., 2006). The instrument illuminates particles with a pulsed green laser as they pass through one focal point of an ellipsoidal mirror. The angularly scattered light is collected by the mirror and focused into a slit to be sensed by a gated image-intensified charge coupled device camera. A major problem

35 with the instrument is the difficulty to measure absolute values of scattering patterns due to various technical factors such as beam power and detector gain fluctuation, particle misalignment, and varying background levels (Walters et al., 2019). The second instrument is an OPC that measures forward and backward scattered light from the illumination of particles using two wavelengths (Szymanski et al., 2009). A major problem with the instrument is the need to set an *ad hoc* scaling factor to relate measurements to particle size and refractive index. The scale factor can change from one measurement to another. The third

40 instrument is the first generation of SPARCLE or SPARCLE 1 (Thomas, 2003). It was a stratospheric instrument designed to retrieve particle size and refractive index based on the pattern of scattering light. Major problems with the instrument were the high dependency of the retrieval results on *a priori* knowledge of the sampled particles and the low efficiency of measurements.

The purpose of this study is to investigate the feasibility of the second generation of SPARCLE or SPARCLE 2 (Peters et al., 2009) which transformed the original design from a stratospheric instrument into one suitable for use in troposphere

45 studies. With dimensions of $60\,cm \times 30\,cm \times 20\,cm$ and weight of about $15\,kg$, SPARCLE 2 is a field-deployable instrument. SPARCLE 2 has two measurement goals. The first goal is to provide size-resolved measurements of particles whose sizes range from $500\,nm$ to $2,500\,nm$. This size range is within the range of the accumulation mode of tropospheric aerosol. The second goal is to measure both particle size and refractive index based on the pattern of scattered light. Particle size and refractive index can be retrieved unambiguously using Mie scattering theory (Mie, 1908) assuming that measured particles are homogeneous

50 spheres. SPARCLE 2 is suitable for ambient measurement since large proportions of ambient particles with sizes between $500\,nm$ and $2,000\,nm$ are either liquid droplets or particles with morphologies that have a dominant liquid phase (Prospero et al., 1983; Sullivan and Prather, 2005; Pinnick et al., 2011).

2 SPARCLE design and system feature

The arrangement of SPARCLE 2's main components is shown in Figure 1. To maximise the collected light, the detectors were

55 placed as close as practical to the sensing volume and no additional optics were employed to collect the scattered light. As shown in the figure, the detectors are located on the either side of the sensing volume. Their axis of symmetry crosses the sensing volume, and is at right angles to both the sample air flow and the illuminating beam. The beam propagates along the

z-axis with the beam polarisation along the y-axis. The two detectors are located at around $6\,\mathrm{mm}$ from the z-axis. While this approach may be prone to stray light, it is preferable due to its simplicity.
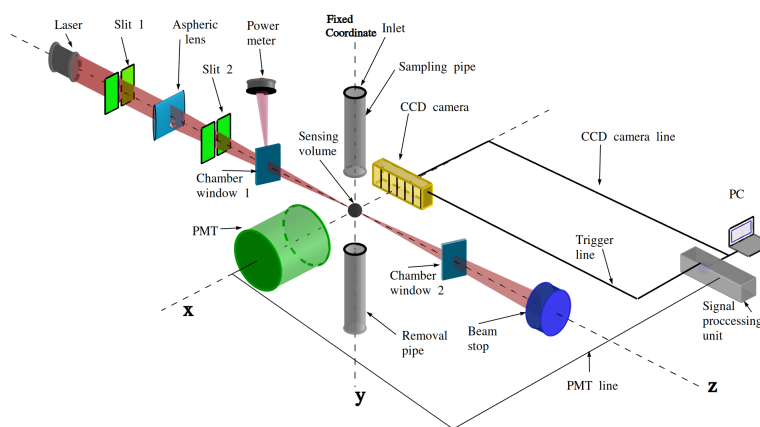
Figure 1. The arrangement of SPARCLE 2's main components. Three vectors are defined by the PMT axis of symmetry, the sampling pipe centre and the central axis of the laser beam. These three vectors form an orthogonal $x - y - z$ fixed coordinate system with the origin at their point of the intersection.

The choice of detectors was influenced by two considerations: first, SPARCLE 2 should be sensitive to particle sizes in the range $500\,\mathrm{nm}$ to $2{,}500\,\mathrm{nm}$, and second, it should be able to measure the scattered light at an angular resolution sufficient to resolve the principal structure of the scattering patterns for these sizes. This was achieved using two coupled detectors. The first detector records if a particle is in the sensing volume. If a particle is present, the second detector measures the pattern of scattered light. The first detector needs the sensitivity to measure light scattered by a $500\,\mathrm{nm}$ particle, and high temporal resolution, much shorter than the transit time of particles in the sensing volume. These requirements lead to the selection of the Electron Tube photomultiplier tube (PMT) model 9124B due to its high conversion efficiency of photons into photoelectrons, its high gain and its short response time. This PMT can detect light with wavelengths between $280\,\mathrm{nm}$ and $680\,\mathrm{nm}$, and its conversion efficiency is around 25% (at $\lambda = 400$ nm). The amplification is up to 10^6 and the response time is $33\,\mathrm{ns}$. The second detector needed to have a high spatial resolution and high photon sensitivity to capture fine details of the light scattering pattern as well as the ability to integrate scattered light over a relatively short period of time (on the order of the transit time of particles in the sensing volume). These requirements were fulfilled by the LC1-USB CCD line camera produced by Thorlabs. The camera contains a $3{,}000$ pixel linear sensor (ILX526A) whose sensitivity to light at a wavelength of $660\,\mathrm{nm}$ is $3{,}000\,\mathrm{V\,lux^{-1}\,s^{-1}}$. The integration time of the CCD camera ranges from $1\,\mathrm{\mu s}$ to $200\,\mathrm{ms}$ with an electronic shutter function. The manufacturer did not specify the quantum efficiency of the line sensor, however an efficiency of 35% (at $\lambda = 650$ nm) was measured by Labusov et al. (2008).

The source of illuminating light was selected based on the need to generate a high intensity and well-collimated beam of light within a narrow wavelength band. Additional considerations were the need for SPARCLE 2 to require low power

and to be compact to facilitate *in situ* measurements. One type of light source that can satisfy these criteria are laser diodes. The choice is a compromise between higher power, shorter wavelength laser diodes which produce a more intense scattering pattern, and the extra complication needed to make the instrument eye-safe. It was decided to use the CPS65AP05-SE laser diode emitting light of wavelength 650 nm and output power around 4 mW. The laser comes in a module with pre-installed collimating lens resulting in a nearly elliptical collimated beam with a major axis of 6 mm and a minor axis of 3 mm. The beam was characterised using a spectrometer and shown to have a maximum intensity at 651.51 nm. The output power of the laser was measured as 3.9 mW and the light was polarised in the major axis of the ellipse.

The sensing volume is determined by the intersection of the laser beam and the air flow exiting the sampling pipe. The volume is a trade-off between maximising the illumination time and minimising coincidence error (having more than one particle illuminated). The elliptical shape of the laser beam was undesirable since it leads to a bigger coincidence error. It was avoided by compressing the laser beam along its major axis resulting in a thin nearly rectangular beam with dimension about $1.5\,\text{mm} \times 0.4\,\text{mm}$. This size provides an illumination time longer than $1,000\,\mu\text{s}$ for particles carried in air at $170 \times 10^{-9}\,\text{m}^3\,\text{s}^{-1}$ from a pipe of radius 0.5 mm. For this configuration the coincidence error is calculated to be less than 15% of true counts when the particle concentration is $1,000\,\text{cm}^{-3}$.

When a particle is in the sensing volume, it is illuminated by the laser beam. The scattering geometry is shown in Figure 2 with the particle as the centre of reference for the scattering. In the figure, the beam intensity is represented by its electric component $\overrightarrow{E}$ and the intensity of the two scattered light components (parallel and perpendicular to the plane of scattering) are denoted by $I_{\parallel}$ and $I_{\perp}$. The scattered light can be calculated using Mie theory assuming a spherical particle. The total scattered light intensity I over a solid angle represented by an area constrained by azimuth angles ϕ_1 & ϕ_2 swept around a sphere constrained by zenith (scattering) angles θ_1 & θ_2 can be expressed as

$$I = \frac{\lambda^2}{4\pi^2} \int\limits_{\phi_1}^{\phi_2} \int\limits_{\theta_1}^{\theta_2} \left[I_{\parallel}(\alpha, m, \theta, \phi) \cos^2 \phi + I_{\perp}(\alpha, m, \theta, \phi) \sin^2 \phi \right] G(\theta, \phi)\, d\theta\, d\phi, \tag{1}$$

where α is a size parameter defined as $\alpha = \frac{\pi d}{\lambda}$ with d as the particle diameter and λ as the wavelength of the illuminating light; m is particle refractive index; $G(\theta, \phi)$ is geometrical factor specific to the instrument's design.

In a particular case where a particle is at the origin, the PMT collects scattered light over a solid angle represented by an arc from $\phi_1 = 40°$ to $\phi_2 = 140°$ swept around a sphere from $\theta_1 = 20°$ to $\theta_2 = 160°$. The responses of the PMT to various particle size were calculated and the results are highly structured as shown in Figure 3. A near linear response can be seen for particles smaller than 1,000 nm. For particles bigger than 1,000 nm, the response generally increases with size but includes resonance peaks where the optical path inside the sphere is a multiple of the wavelength. Similarly, the 3,000 pixels of the CCD camera measure scattering light from $\theta_1 = 37°$ to $\theta_2 = 144°$ and the azimuth angle of each pixel can be taken as $\phi = 90°$. The solid angle of each pixel is typically around 8×10^{-7} sr. This solid angle is sufficiently small that the variation of θ and ϕ in each pixel can be omitted. Figure 4 shows the scattering angle as a function of CCD pixels. The expected responses of the CCD camera to particles with three different sizes: 1,000 nm, 2,000 nm and 3,000 nm and a refractive index of 1.59 were calculated. The results were three distinctive patterns as shown in Figure 5.

Atmospheric
Measurement
Techniques
Open Access

EGU

Discussions
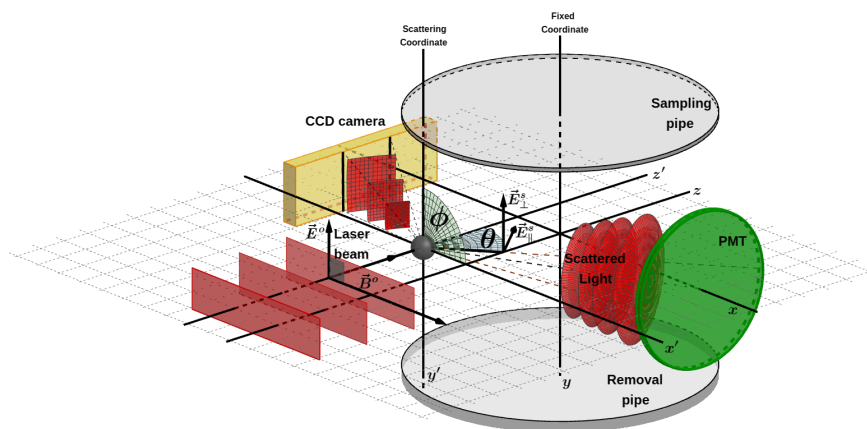
Figure 2. The geometry of light scattering in the sensing volume. Two coordinates are shown in the figure: fixed and scattering coordinates. The laser beam propagated along the z' axis, and polarised parallel to the y' axis. In a particular case when the scattering plane is on the $x - z$ plane, $\overrightarrow{E}_\parallel^s$ is zero.
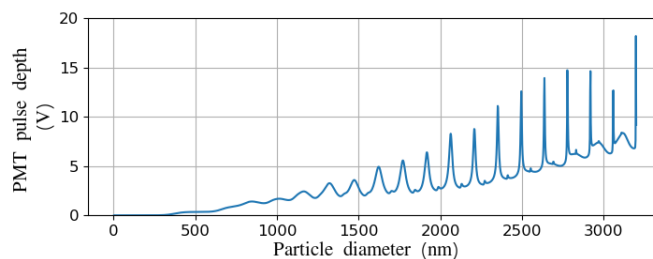
Figure 3. The expected PMT responses to various particle sizes with a refractive index of 1.59. The responses are PMT pulse depth with the depth calculated relative to background level. The unit of PMT responses is Volt as a result of an electrical current conversion using a $150\,\Omega$ load resistor. The voltage of the load resistor was then amplified by a factor of 550.

The detection limit of SPARCLE 2 can be estimated by considering two noise sources: the PMT dark current and the Rayleigh scattering of the laser beam by the air between chamber window 1 and 2. The dark current was specified by the manufacturer as 0.3 nA when no photons fall on the PMT window. The current then corresponds to a PMT output of 0.1 mV. In the calculation of the Rayleigh scattering, only single scattering by air molecules ($d_{N_2} = 0.3\,\text{nm}$, $m = 1.0003$) was considered as higher order scattering was negligible. Also, the beam intensity was assumed to be constant during its propagation in the chamber. The number of the scattering air molecules can be derived by multiplying air density (at an atmospheric pressure of 1012 hPa and a temperature of $20°$ C) by the volume of the laser beam in the chamber. The calculation resulted in the intensity of scattering light corresponding to the PMT output less than 0.1 mV. To illustrate, PMT responses to particle size are plotted in

115
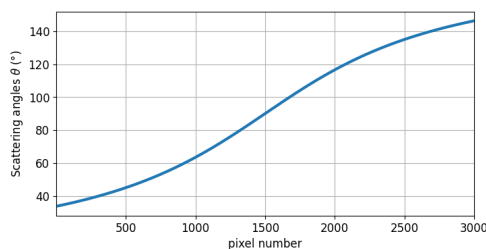
Figure 4. The mapping of the pixels to scattering angles for a special case when the reference centre of scattering and fixed coordinates coincide.
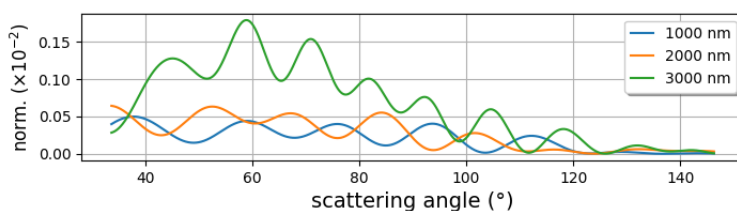
Figure 5. The responses of the CCD camera to three different particle sizes. The integration time was $1,000\,\mu s$. The responses were calculated by converting the optical power of scattered light into volts with the conversion range between $0\,V$ and $-2.3\,V$ as specified by the line sensor manufacturer. The CCD camera presents the output by normalising the volts into a range from 0 to 1 which linearly corresponds to a range of $0\,V$ down to $-2.3\,V$.

Figure 6 along with the noise. As shown in the figure, signal-to-noise ratio *SNR*, calculated by dividing PMT outputs and total
120 noise, is less than one and greater than 100 when measuring particles smaller than $150\,nm$ and bigger than $300\,nm$, respectively.

The interference of noise on the CCD camera measurements was also analyzed. The manufacturer specifies that typical dark voltage generated by the CCD line sensor is $2.5\,mV$. The normalised output for this voltage is around 10^{-3}. The Rayleigh noise was calculated based on the scattering model similar to that for the PMT measurements. The calculation was done for a pixel located in the scattering angle of $90°$. For simplicity, the Rayleigh noise at this pixel was generalised for all pixels. The result
125 indicates that the Rayleigh noise for a pixel is in the order of 10^{-4}. The combination of the two noise sources is still small relative to expected scattering patterns shown in Figure 5.

The Fresnel equations are used to correct the output of the CCD camera due to the presence of the glass window in front of the sensor. The correction is a function of the polarisation, the incident angle of the light and the refractive index of the glass (specified as 1.5 by the manufacturer). An example of the effect of the glass is shown in Figure 7. The glass window reduces
130 the intensity of the scattering light by $7\,\%$ - $26\,\%$.

A final aspect in SPARCLE 2's design was the air sampling, transport and exhaust system. Ambient air needs to be delivered to the sensing volume with minimal loss in the particle concentration. This is achieved using a 3 cm long pipe with the diameter of 0.5 mm. Laminar air flow is obtained by using flow rates less than $500 \times 10^{-19}\,\mathrm{m^3 s^{-1}}$ (giving a Reynolds number less than 40). To avoid double counting, particles need to be removed immediately after they leave the sensing volume. To keep the

Atmospheric
Measurement
Techniques
Discussions
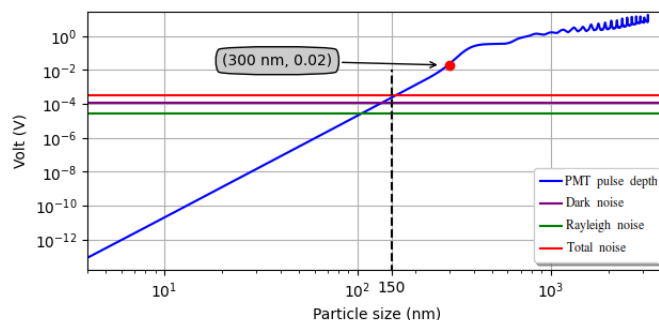
Figure 6. The response of the PMT compared with the Rayleigh, dark and total noise. For clarity, the total noise in the figure is multiplied by a factor of 2. The-signal-to-noise ratio equal to one is indicated by a dashed line while the ratio equal to around 100 is indicated by a red dot.
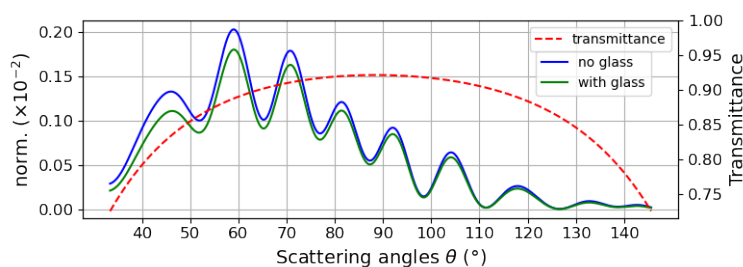
Figure 7. The effect of the glass installed in the CCD camera on the intensity of light scattered by a particle with a diameter of 3,000 nm and a refractive index of 1.59. The intensities with and without the glass are shown as blue and green lines. The transmittance through the glass is plotted as a dashed red line using the scale on the secondary vertical axis. The transmittance peaks at a scattering angle of $90°$.

135   design simple, no active flushing or sheath flow has been used. However, if the separation between the pipes was too small then reflection from the pipes increased background noise. Experiments were performed that identified an optimum gap of 1 mm. The streamlines of air flow through the sampling pipe, the sensing volume, and the removal pipe were simulated using OpenFoam software. The results indicates that the air velocity in the pipes is distributed quadratically while that in the sensing volume is distributed normally with respect to the symmetry axis of the sampling pipe. The loss of particles when sampling air

140   through the sampling pipe was calculated using Particle Loss Calculator (PLC) software. The results indicate that the loss is less than 10% (sampling efficiency > 90%) when sampling particles with sizes between 500 nm and 1,800 nm. When sampling particles bigger than 1,800 nm, the efficiency decreases as the size increases. For example, the efficiency can be down to 50% and 30% when sampling particle size of 6,000 nm and 10,000 nm, respectively.

Atmospheric
Measurement
Techniques
Discussions
Open Access
EGU

3 SPARCLE 2 Characterisation

3.1 Dark and background noise in the scattering chamber

The dark and background were measured with no particles in the sensing volume with the laser off and on, respectively. The PMT outputs from the dark measurements were shifted to +4.6 V to optimise the data acquisition system measurement range between -5 V and +5 V. Note that the PMT outputs are lower for brighter scattering light. The dark measurements can be seen as blue dots in Figure 8.a. Meanwhile, the dark measurements were also performed by the CCD camera and the results are plotted as blue dots in Figure 8.b. Then, the laser was switched on to measure the background. The results of the measurements by the PMT and the CCD camera are shown as red dots in Figures 8.a and 8.b, respectively. As shown in Figure 8.a, the mean and the standard deviation of the background were 3.1 V and 0.06 V, respectively. The standard deviation is higher than the expected noise from Rayleigh and Dark noise indicating the presence of other noise sources. The other sources can be identified based on the CCD camera outputs. The outputs were higher for pixels closer to the sampling pipe indicating that there was beam reflection by the pipe. Also shown in Figure 8.a, the background variation could be 0.4 V. Due to the variation, a threshold level of PMT outputs was set to be 0.4 V lower than the mean background to differentiate between background variation and scattering signals.
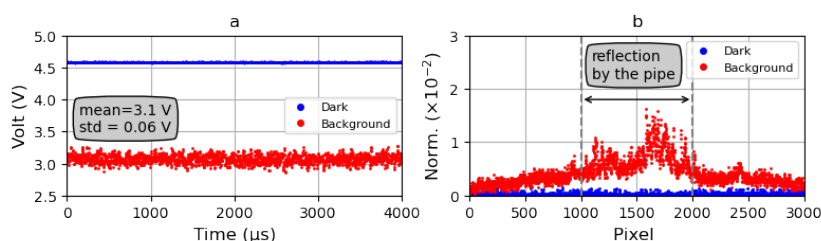
Figure 8. The dark and background measurements by the PMT (a) and the CCD camera (b), respectively.

3.2 SPARCLE 2 measurement acceptance criteria

Once particles are detected, measured scattered light should fulfil two criteria to qualify for further analysis. First, the PMT outputs should be higher than the lower limit of the acquisition system: -5.0 V. Second, the CCD camera outputs should contain sufficient scattering signals relative to the background variance. Scattering signals, S, at a pixel j can be calculated using the output $\mathcal{V}_j$ and the background $\overline{\mathcal{V}}_j^{\mathrm{b}}$ as

$$S_j = \mathcal{V}_j - \overline{\mathcal{V}}_j^{\mathrm{b}}. \tag{2}$$

Atmospheric
Measurement
Techniques
Discussions

Open Access

The value of $\overline{\mathcal{V}}_j^{\text{b}}$ was found from the average of 200 background measurements. The background variance, σ^2, was calculated

165 from:

$$\sigma^2 = \frac{1}{N-1} \sum_{j}^{N} \left(\mathcal{V}_j^{\text{b}'} - \overline{\mathcal{V}}_j^{\text{b}} \right)^2, \tag{3}$$

where N is the number of the pixels; $\mathcal{V}_j^{\text{b}'}$ is a single background measurement. The quality of the scattering signal was indicated by the signal-to-noise ratio *SNR* defined as

$$SNR = \frac{1}{N-1} \frac{\sum_{j}^{N} S_j^2}{\sigma^2}. \tag{4}$$

170 The limiting value of *SNR* was estimated from four samples. Figure 9 shows that a scattering pattern is discernible when the SNR is greater than 3.31. To give a small margin of safety that SNR value of 4.2 was selected as the lower measuremnt limit.
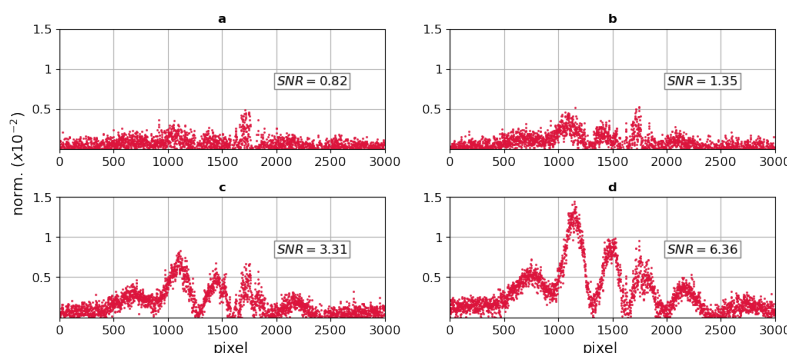
Figure 9. Four samples of S used to determined the limit of *SNR* for the acceptance criteria.

3.3 The beam distribution across the x-y plane in the sensing volume

Two approaches were used to infer the beam distribution across the x-y plane in the sensing volume. The first was by measuring the distribution along the x-axis and the second was by deducing the distribution along the y-axis using the shape of PMT

175 responses. The first was done by a bespoke profiler composed of a linear photo-diode array (TSL201R-LF) and the results are shown in the top of Figure 10. Meanwhile, the shape of PMT responses are shown in the right of the figure. The shape is a skewed Gaussian with the standard distribution of 0.1 mm. The two approaches are combined to infer the distribution across the x-y plane and the result is shown in the bottom left of the figure.
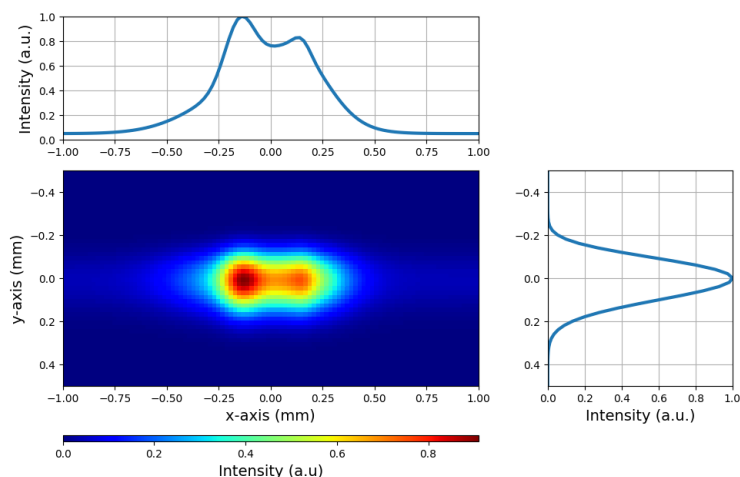
Figure 10. Two-dimensional intensity distribution of the beam across the x-y plane in the sensing volume. The projections of the intensity at the x and y axis are shown at the top and right figure, respectively. To note, the beam propagates through the plane. The unit for the intensities is arbitrary unit (a.u).

3.4 Particle detection efficiency

180   The efficiency of SPARCLE to detect a particle $\eta(d, m)$ can be calculated by considering the spatial distribution of the beam and particle position in the sensing volume. A simple model of the position was developed: particles flow through a vertical path parallel to the y-axis with the same velocity of the air in which they are suspended. The probability of particles flowing at a particular vertical path $f(x, z)$ is calculated as the ratio between air flow rate at the path and SPARCLE 2 sampling flow rate. To illustrate, $f(x, z)$ calculated with the sampling flow rate of $170 \times 10^{-9} \, \mathrm{m^3 \, s^{-1}}$ and is shown in Figure 11.a while the beam

185   distribution over the same plane is shown in Figure 11.b. To calculate $\eta(d, m)$, the plane was discretized as a grid with uniform spacing Δx and Δz, and $f(x, z)$ was assumed to be homogeneous over an area $\Delta x \Delta z$. Grid points where particles can be detected and the corresponding responses qualify for the acceptance criteria are denoted as (x_i, z_i). The detection efficiency can be calculated as

$$\eta(d, m) = \sum_i f(x_i, z_i) \Delta x \Delta z. \tag{5}$$
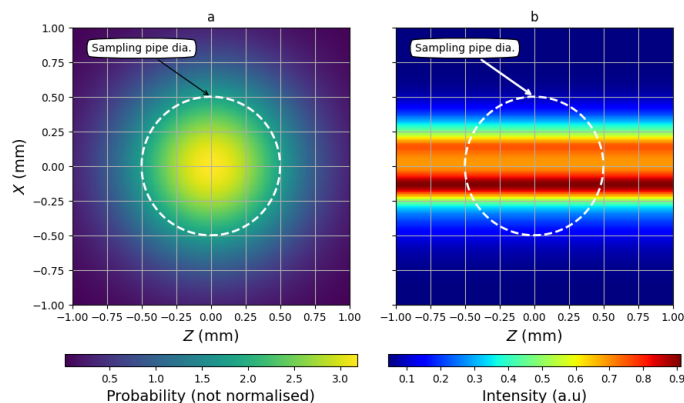
Figure 11. The distributions of particle position probability (a) and the beam intensity (b) across the x-z plane in the sensing volume. As shown in the figure, particles are highly likely to pass around the symmetrical axis of the sampling pipe. The scale of the probability is not normalised and the scale of the beam intensity distribution is an arbitrary unit. The projection of the sampling pipe in the plane is shown by white dashed line. To note, the flow of particles is through the plane.

3.5 SPARCLE 2 measurement efficiency

The measurement efficiency is the combination of SPARCLE 2 sampling and detection efficiency. The measurement efficiency was calculated and is shown in Figure 12. In the figure, the efficiencies are colour-coded from blue to red colours corresponding to low to high efficiencies. As shown in the figure, the efficiencies are highly non-linear functions of particle size and refractive index. Low efficiencies can be seen when measuring particles smaller than 1,600 nm. These low efficiencies are due to both the thresholds of 0.4 V and the *SNR* limit of 4.2. Nearly zero probabilities are seen for measuring particles smaller than 800 nm. This size can be regarded as the limit detection of SPARCLE 2. Low efficiencies can also be seen on the top right of the figure that roughly corresponds to measuring particles bigger than 6,100 nm and refractive index bigger than 1.40. These low efficiencies are due to the combination of low efficiencies to sampling particles bigger than 6,100 nm and the saturation of PMT pulses due the lower limit of the acquisition system. Meanwhile, SPARCLE 2 is highly efficient to measure particles between 1,600 nm and 6,100 nm.
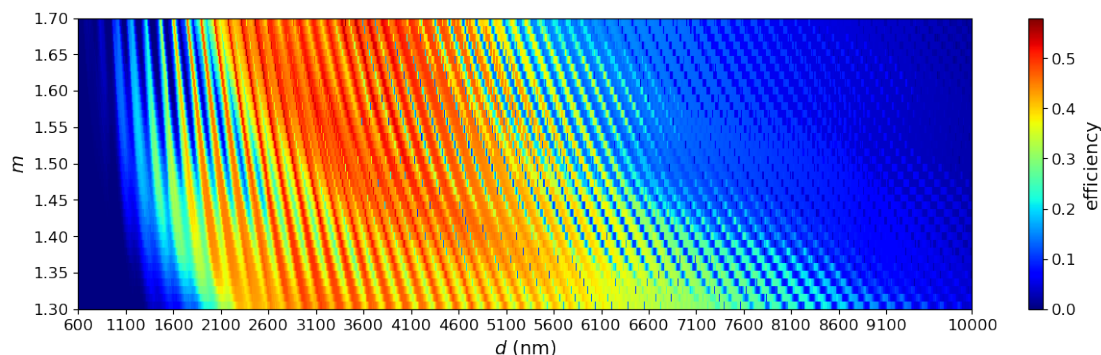
Figure 12. The measurement efficiency of SPARCLE 2.

3.6 SPARCLE 2 Validation

SPARCLE 2 was validated using four monodisperse test aerosols. The aerosols were generated by nebulizing suspensions containing polystyrene latex (PSL) beads into droplets, and drying the droplets to produce solid aerosols. The nebulization was done using TOPAS ATM 220. The suspensions were prepared by diluting stock solutions containing PSL beads. The details of the stock solutions are listed in Table 1. During the validation, the size distributions of the test aerosols were also measured by a manufacturer calibrated GRIMM 1.108 OPC and the results show that the distributions peaked around the sizes specified by the manufacturers with additional particles smaller than 600 nm. The smaller particles could be formed by the condensation of surfactant added by the manufacturers to stabilise the stock solutions. The relative humidity of the sample air and the power of the laser beam were also monitored. It was found that the humidity was lower than 25% indicating that the droplets were perfectly dried. Also, the laser power was relatively stable with a variation around 1% of the mean power.

Table 1. The mean and the standard deviation of PSL bead size contained in the four stock solutions. The bead refractive index is 1.59.

No.	Product	Suppliers	Mean size & std	
			(nm)	(%)
1	LB11	Sigma-Aldrich	1,100	5
2	42744	ThermoFisher Sc.	1,800-2,200	3
3	5200A	Duke Scientific	2,000	5
4	LB30	Sigma-Aldrich	3,000	5

The retrieval of particle properties is based on a forward model of SPARCLE $\mathbf{F}(\mathbf{x})$ that predicts the CCD camera and PMT response as a function of the particle state $\mathbf{x}$, i.e. the particle's position in the x-z plane, its size and its refractive index. Given the SPARCLE response $\mathbf{y}$, the particle state is the vector of values that minimises

$$\chi^2 = \frac{1}{v}[\mathbf{y} - \mathbf{F}(\mathbf{x})]^{\mathrm{T}}\mathbf{S}^{-1}[\mathbf{y} - \mathbf{F}(\mathbf{x})], \tag{6}$$

215   where υ is the degrees of freedom and $\mathbf{S}$ is the measurement uncertainty covariance matrix (Rodgers, 2000). In this study, the value of $\chi^2 < 4.0$ was used to indicated a good fit. For computational efficiency the forward model used a look-up table covering the domain

- particle-position from -1.00 mm to +1.00 mm in steps of 0.01 mm,

- size from 600 nm to 10,000 nm in steps of 1 nm,

220   - refractive index from 1.30 to 1.70 in steps of 0.01.

To illustrate this approach the PMT and CCD response to a particle of size 1,800 nm is shown in Figure 13 along with the forward modelled values (at the minimum). The retrieved particle state is given as part of Figure 13b.
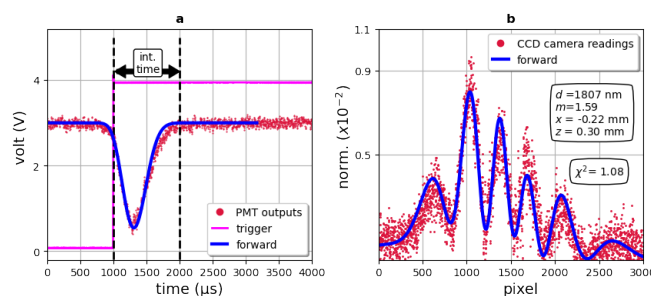
Figure 13. An example of SPARLCE 2 responses to a PSL particle of 1,800 nm. The outputs of the PMT and the CCD camera are shown in (a) and (b), respectively. In (a), the integration time when the CCD camera collected scattered light is indicated. The integration time is started by the increasing of trigger signals generated when PMT outputs lower than the threshold. The blue lines in (a) and (b) are the forward model of SPARCLE 2 responses calculated using parameters indicated in (b).

To validate the method 10,000 aerosols for each test sample were recorded and particle properties determined . The validation results are summarised in Figure 14. In the figure, the retrieved size and refractive index are plotted as a function of the sizes stated by the manufacturers. The dashed lines mark the values stated by the manufacturers. The results indicate that the largest 225 deviation of the retrieved particle size is 13% for particles of size 1,100 nm. For the bigger particles, the deviations are less than 3%. The deviation of retrieved particle refractive index is less than 1.25%.
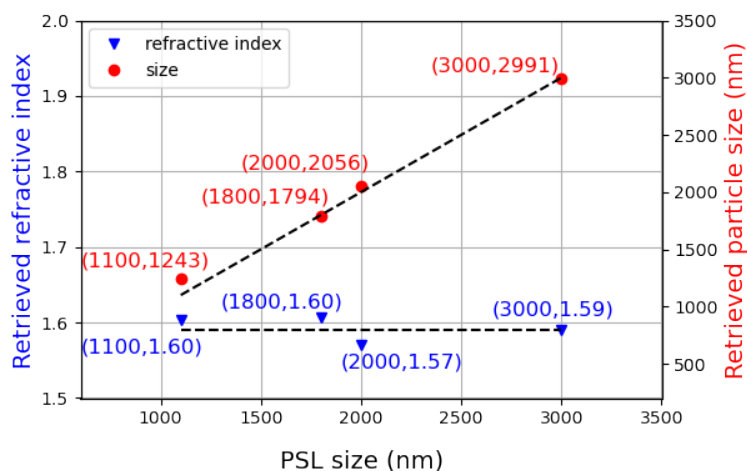
Figure 14. The sizes and refractive indices retrieved from SPARCLE 2 responses to the four test aerosols. The sizes are plotted as red dots with the scale on the right while the refractive indices are plotted as blue triangles with the scale on the left. The dashed lines mark the expected values of retrieved size and refractive index. To note, the uncertainties of the PSL size are less than 5% of the size as listed in Table 1 while the uncertainty of PSL refractive index are not published.

4 SPARCLE ambient measurements and results

As a further test, SPARCLE 2 was used to measure ambient aerosol adjacent to the Atmospheric Physics Building at the
230 University of Oxford. The measurements were made for around 40 hours from 31 July 2021 to 1 August 2021. The ambient was also measured by the GRIMM OPC. Both instruments were put next to an open window of the laboratory. The humidity during the measurements were between 50% to 60%.

In this experiment, 10,000 responses were made. Of these only 676 responses fitted with the forward models. The results are shown in Figure 15. As shown in the figure, the raw distributions of particle size and refractive index are multi-modal. There
235 are at least two bias that lead to this distribution:the non-linearity of the measurement efficiency and the non-absorbing particle assumption used in the forward model. The first bias can be corrected using the measurement efficiency. Meanwhile, a further study is needed to correct the second. When corrected for measurement efficiency the particle size distribution is shown as red bars in Figure 16. As seen in the figure, the corrected size distribution is the same order of that measured by the GRIMM OPC for the size range within the working range of SPARCLE 2. The efficiency was also used to correct the distribution of particle
240 refractive index. Figure 17 shows the aerosol refractive index was spread between 1.3 and 1.7 with peaks at 1.40 and 1.50. To the authors knowledge, this is the first ambient measurement of a particle refractive index distribution.

One way to evaluate the particle refractive index distribution is to consider the most abundance aerosol components suspending around Oxford. A series of aerosol measurements were done at Harwell, 20 km south of Oxford, in 2014 (Vieno et al., 2016). The results indicate that the most abundant aerosol components are NO_3^-, NH_4^+ and SO_4^{2-}. Aerosols that contain those
245 components can be droplets of NH_4NO_3, $(NH_4)_2SO_4$ and NH_4HSO_4. At the current time, there are no data of the refractive

index of NH_4NO_3 droplets in the visible range. The refractive indices of NH_4NO_3 and $(NH_4)_2SO_4$ droplets as functions of humidity were calculated by Tang (Tang and Munkelwitz, 1994) and the results are between 1.41 and 1.43 when the humidity between 50% and 60%. This range of refractive index partly overlaps with the range of the peak of the refractive index distribution shown in Figure 17 suggesting that a large number of NH_4NO_3 and $(NH_4)_2SO_4$ droplets were sampled during the

250 ambient measurements. While a large proportion of particles with the refractive index lower than 1.40 as seen in Figure 17 can be regarded as water droplets with various purity, those with refractive index bigger than 1.62 still can not be unambiguously identified.
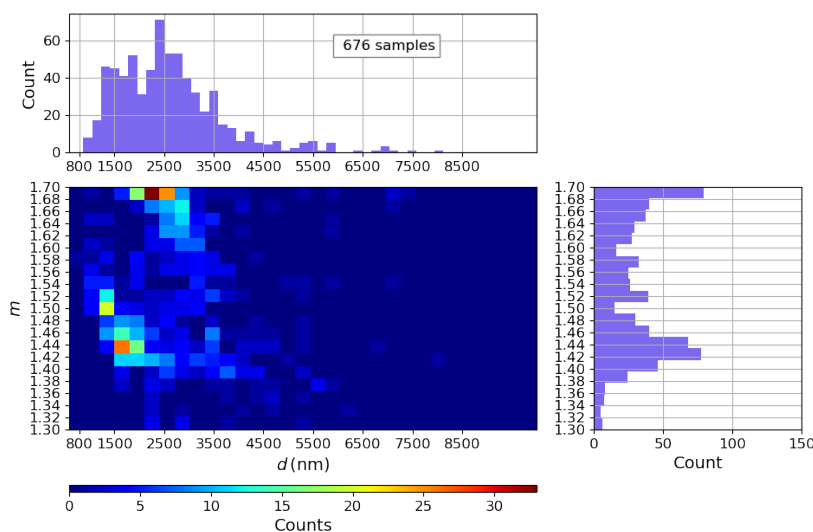
Figure 15. The distribution of particle size (top figure) and refractive index (right figure) in Oxford as measured by SPARCLE 2.
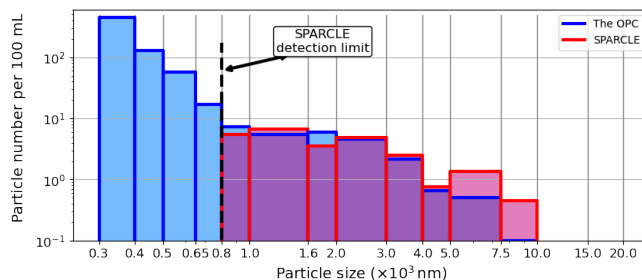
Figure 16. The size distribution of Oxford ambience as measured by the OPC (blue bars) and SPARCLE 2 (red bars).

Atmospheric
Measurement
Techniques
Discussions
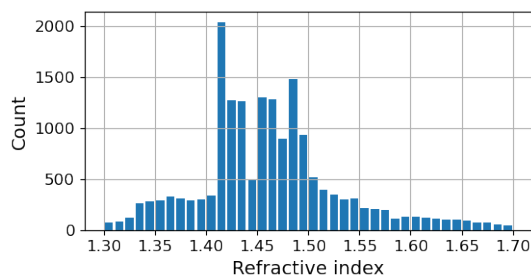
Figure 17. The corrected particle refractive index distribution of Oxford ambience.

5 Conclusions

The design of SPARCLE 2 and its characterisation has been discussed. The design indicates that SPARCLE 2 is able to measure
particles bigger than 300 nm assuming that the noise in the scattering chamber is from dark current and Rayleigh scattering. In
the characterisation, another source of noise was detected and it generated background noise bigger than that from dark current
and Rayleigh scattering. To differentiate between the background and scattering signals, a threshold was applied that raised
the limit detection to be 800 nm. The sampling and detection efficiencies were used to calculated the measurement efficiency.
The results indicate that SPARCLE 2 is highly efficient to measure particles between 1,600 nm and 6,100 nm. SPARCLE 2
was then validated using four test aerosol particles whose size and refractive index were known. Based on the specification
provided by the manufacturer, the mean of the particle diameters were 1,100 nm, 1,800 nm, 2,000 nm, and 3,000 nm and the
particle refractive index is 1.59. The validation results indicate that the deviation of SPARCLE 2's measurements from the
size stated by the manufacturer is 13% for particle size of 1,100 nm. For the bigger particles, the deviation is less than 3%.
Meanwhile, the deviation of particle refractive index is less than 1.25% from that stated by the manufacturer. SPARCLE was
used to measure the size and refractive index of aerosols in ambient air. The size distributions measured by SPARCLE 2 was in
the same order to that measured by the OPC within the working range of SPARCLE 2. While, the refractive index distribution
were inline with the most abundance aerosol composition around Oxford which were NO_3^-, NH_4^+ and SO_4^{2-}.

16

Competing interests. No conflict interest were identified.

Atmospheric
Measurement
Techniques
Discussions

References

Aptowicz, K. B., Pinnick, R. G., Hill, S. C., Pan, Y. L., and Chang, R. K.: Optical scattering patterns from single urban aerosol particles at Adelphi, Maryland, USA: A classification relating to particle morphologies, J. Geophys. Res. Atmos., 111, https://doi.org/10.1029/2005JD006774, 2006.

Boucher, O. and Lohmann, U.: The sulfate-CCN-cloud albedo effect: A sensitivity study with two general circulation models, Tellus B: Chemical and Physical Meteorology, 47, 281–300, https://doi.org/10.3402/tellusb.v47i3.16048, 1995.

Brook, R. D., Franklin, B., Cascio, W., Hong, Y., Howard, G., Lipsett, M., Luepker, R., Mittleman, M., Samet, J., Smith, S. C., and Tager, I.: Air pollution and cardiovascular disease, Circulation, 109, 2655–2671, https://doi.org/10.1161/01.CIR.0000128587.30041.C8, 2004.

Brook, R. D., Rajagopalan, S., Pope, C. A., Brook, J. R., Bhatnagar, A., Diez-Roux, A. V., Holguin, F., Hong, Y., Luepker, R. V., Mittleman, M. A., Peters, A., Siscovick, D., Smith, S. C., Whitsel, L., and Kaufman, J. D.: Particulate matter air pollution and cardiovascular disease: an update to the scientific statement from the American Heart Association, Circulation, https://doi.org/10.1161/cir.0b013e3181dbece1, 2010.

Erlick, C., Ynelisa, Abbatt, J. P., and Rudich, Y.: How different calculations of the refractive index affect estimates of the radiative forcing efficiency of ammonium sulfate aerosols, Journal of the Atmospheric Sciences, 68, 1845–1852, https://doi.org/10.1175/2011JAS3721.1, 2011.

IARC: Air pollution and cancer, Tech. rep., World Health Organization, Lyon, https://www.iarc.who.int/wp-content/uploads/2018/07/AirPollutionandCancer161.pdf, 2013.

IPCC: Climate Change 2014: Synthesis Report, Tech. rep., Geneva, http://www.ipcc.ch., 2014.

Labusov, V. A., Selyunin, D. O., Zarubin, I. A., and Gallyamov, R. G.: Measuring the quantum efficiency of multielement photodetectors in the spectral range between 180 and 800 nm, Optoelectronics, Instrumentation and Data Processing, 44, 19–26, https://doi.org/10.3103/s8756699008010044, 2008.

Mie, G.: Beiträge zur optik trüber medien, speziell kolloidaler metallösungen, Annalen der Physik, 330, 377–445, https://doi.org/10.1002/andp.19083300302, 1908.

Myhre, G., Samset, B. H., Schulz, M., Balkanski, Y., Bauer, S., Berntsen, T. K., Bian, H., Bellouin, N., Chin, M., Diehl, T., Easter, R. C., Feichter, J., Ghan, S. J., Hauglustaine, D., Iversen, T., Kinne, S., Kirkevåg, A., Lamarque, J.-F., Lin, G., Liu, X., Lund, M. T., Luo, G., Ma, X., Van Noije, T., Penner, J. E., Rasch, P. J., Ruiz, A., Seland Øand Skeie, R. B., Stier, P., Takemura, T., Tsigaridis, K., Wang, P., Wang, Z., Xu, L., Yu, H., Yu, F., Yoon, J.-H., Zhang, K., Zhang, H., and Zhou, C.: Radiative forcing of the direct aerosol effect from AeroCom Phase II simulations, Atmos. Chem. Phys, 13, 1853–1877, https://doi.org/10.5194/acp-13-1853-2013, 2013.

Peters, A., Dockery, D. W., Muller, J. E., and Mittleman, M. A.: Increased particulate air pollution and the triggering of myocardial infarction, Circulation, https://doi.org/10.1161/01.CIR.103.23.2810, 2001.

Peters, D., Grainger, D., and Smith, A.: Local air quality, http://www.icao.int/environmental-protection/Pages/local-air-quality.aspx, 2009.

Pinnick, R., Pan, Y., S.C., H., Aptowicz, B., and Chang, R.: Laser-induced fluorescence spectra and angular elastic scattering patterns of single atmospheric aerosol particles, in: Fundamental and Applications in Aerosol Spectroscopy, edited by Signorell, R. and Reid, J., Taylor {&} Francis, New York, 2011.

Prospero, J. M., Charlson, R. J., Mohnen, V., Jaenicke, R., Delany, A. C., Moyers, J., Zoller, W., and Rahn, K.: The atmospheric aerosol system: An overview, Rev. Geophys., 21, 1607, https://doi.org/10.1029/RG021i007p01607, 1983.

Rodgers, C.: Inverse Methods for Atmospheric Sounding, World Scientific Publishing Co., 2000.

Atmospheric
Measurement
Techniques
Discussions

Open Access

EGU

Sullivan, R. C. and Prather, K. A.: Recent advances in our understanding of atmospheric chemistry and climate made possible by on-line

315   aerosol analysis instrumentation, Analytical Chemistry, https://doi.org/10.1021/ac050716i, 2005.

Szymanski, W. W., Nagy, A., and Czitrovszky, A.: Optical particle spectrometry-Problems and prospects, Journal of Quantitative Spectroscopy & Radiative Transfer, 110, 918–929, https://doi.org/10.1016/j.jqsrt.2009.02.024, 2009.

Tang, I. N. and Munkelwitz, H. R.: Water activities, densities, and refractive indices of aqueous sulfates and sodium nitrate droplets of atmospheric importance, J. Geophys. Res. Atmos., 99, 18 801–18 808, https://doi.org/10.1029/94JD01345, 1994.

320 Thomas, G.: A new instrument for atmospheric aerosol measurement, Ph.D. thesis, University of Canterbury, 2003.

Valenzuela, A., Reid, J. P., Bzdek, B. R., and Orr-Ewing, A. J.: Accuracy required in measurements of refractive index and hygroscopic response to reduce uncertainties in estimates of aerosol radiative forcing efficiency, J. Geophys. Res. Atmos., 123, 6469–6486, https://doi.org/10.1029/2018JD028365, 2018.

Vieno, M., Heal, M. R., Twigg, M. M., MacKenzie, I. A., Braban, C. F., Lingard, J. J. N., Ritchie, S., Beck, R. C., Móring, A., Ots, R., Marco,

325   C. F. D., Nemitz, E., Sutton, M. A., and Reis, S.: The UK particulate matter air pollution episode of March-April 2014: more than Saharan dust, Environmental Research Letters, 11, 44 004, https://doi.org/10.1088/1748-9326/11/4/044004, 2016.

Walters, S., Zallie, J., Seymour, G., Pan, Y.-L., Videen, G., and Aptowicz, K. B.: Characterizing the size and absorption of single nonspherical aerosol particles from angularly-resolved elastic light scattering, Journal of Quantitative Spectroscopy & Radiative Transfer, 224, 439–444, https://doi.org/10.1016/j.jqsrt.2018.12.005, 2019.

330 WHO: Review of evidence on health aspects of air pollution: REVIHAAP project technical report, Tech. rep., World Health Organization. Regional Office for Europe, Bonn, https://www.euro.who.int/{_}{_}data/assets/pdf{_}file/0004/193108/REVIHAAP-Final-technical-report-final-version.pdf, 2013.

Zarzana, K. J., Cappa, C. D., and Tolbert, M. A.: Sensitivity of aerosol refractive index retrievals using optical spectroscopy, Aerosol Science and Technology, 48, 1133–1144, https://doi.org/10.1080/02786826.2014.963498, 2014.